INSTITUTE OF PHYSICS PUBLISHING JOURNAL OF PHYSICS D: APPLIED PHYSICS

J. Phys. D: Appl. Phys. **37** (2004) 770–773 PII: S0022-3727(04)70837-2

Phase-sensitive high-speed THz imaging

Toshiaki Hattori, Keisuke Ohta, Rakchanok Rungsawang and Keiji Tukamoto

Institute of Applied Physics, University of Tsukuba, 1-1-1 Tennodai, Tsukuba, Ibaraki, 305-8573 Japan

E-mail: hattori@bk.tsukuba.ac.jp

Received 23 October 2003
Published 11 February 2004
Online at stacks.iop.org/JPhysD/37/770 (DOI: 10.1088/0022-3727/37/5/020)

Abstract
Phase-sensitive high-speed imaging of terahertz (THz) radiation was achieved by introducing the optical heterodyne detection method to high-speed electro-optic sampling of THz images. Intense THz pulses obtained from a large-aperture photoconductive antenna were used as the source. The electric field distribution on the focal plane of focused half-cycle THz pulses was observed using the apparatus. Annular spatial profiles were observed in the time-dependent images. The frequency-dependent distribution calculated by means of Fourier transformation showed almost diffraction-limited focusing.

1. Introduction

Imaging with terahertz (THz) radiation has been attracting attention because the radiation in this frequency region has only recently become available for imaging, thus allowing phase-sensitive detection to be possible in principle [1]. It takes a long time to obtain images using relatively weak THz radiation since spatial scanning of the THz beam is required, which can prohibit applications in the real world. Simultaneous detection of two-dimensional data using a charge coupled device (CCD) camera has made possible high-speed THz imaging [2, 3], where no spatial scanning is needed. We have reported previously a fast THz imaging method using high-power THz pulses generated from large-aperture photoconductive antennas [3], where electro-optic (EO) sampling measurements of the two-dimensional spatial distribution of THz intensity were achieved using a large-area EO crystal, an expanded probe beam, and a CCD camera [3]. In this method, however, the polarizer and the polarization analyser were oriented perpendicular to each other, and the spatial distribution of the intensity, or the squared electric field, was obtained. The most commonly adopted balanced detection method used in EO sampling [4, 5], which directly measures the electric field, is virtually impossible in image detection using a CCD camera.

The field-linear detection method of nonlinear optical signals using the polarization change of the probe light was first developed by Eesley and Levenson [6, 7] for measurements of the Raman-induced Kerr effect. They introduced the optical heterodyne detection (OHD) method, where the optical field generated by the nonlinear optical processes is heterodyne detected by a local oscillator, which is a phase-shifted fraction of the probe light. The OHD technique has since been applied to several schemes aimed at detecting optical Kerr effects [8–10]. Jiang *et al* [11] introduced this technique to THz field detection using the EO sampling method and derived the optimal bias point under the existence of background light.

In this report, we applied for first time the OHD method for the high-speed imaging of the two-dimensional spatial distribution of a THz field using a CCD camera. A time-dependent spatial distribution of the electric field of focused half-cycle THz pulses was obtained from the measurements. Annular spatial profiles of the field at time regions slightly apart from the peak were verified, which were first observed using the THz intensity imaging set-up [3]. Fourier analysis of the temporal profile of the field at each position showed the frequency-resolved two-dimensional spatial profile of the field, which is not possible using the intensity images.

2. Experimental set-up

The experimental set-up is shown in figure 1, which is based on a previously described set-up [3, 12–14]. A regeneratively amplified Ti : sapphire laser provides 800 nm pulses with a duration of 150 fs at a repetition rate of 1 kHz. The major part of the output was used to pump a large-aperture GaAs photoconductive antenna with a 3 cm gap between the electrodes. The THz radiation emitted in the transmitted direction was focused by an off-axis parabolic mirror with a focal length of 152.4 mm. With this set-up, almost half-cycle pulses with a subpicosecond duration are obtained [3, 14].

The two-dimensional spatial distribution of the THz field on the focal plane was measured by means of EO sampling with a 1-mm-thick $\langle 110 \rangle$ ZnTe crystal. The ZnTe crystal had an active area of 18 mm (horizontal) $\times$ 20 mm (vertical). A 1/5 image of the spatial profile of the THz radiation on the crystal position was obtained using the CCD camera. A quarter-wave plate was inserted for electric field detection as described in figure 2.

The configuration of the polarizer, EO crystal, wave plate, and polarization analyser in the OHD method is compared with that of the balanced detection method shown in figure 2. In the OHD set-up, the quarter-wave plate has an axis parallel to the incident light polarization. The analyser is rotated by a small angle, δ, from the crossed orientation. The intensity of the probe light transmitted through this set-up can be expressed as [11]

$$I = I_0[\eta + \sin^2(\delta + \theta)], \tag{1}$$

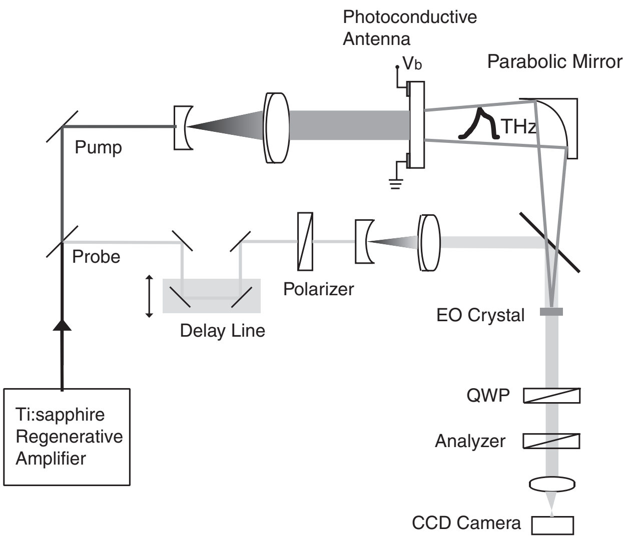

Figure 1. Schematic of the experimental set-up. QWP: a quarter-wave plate.

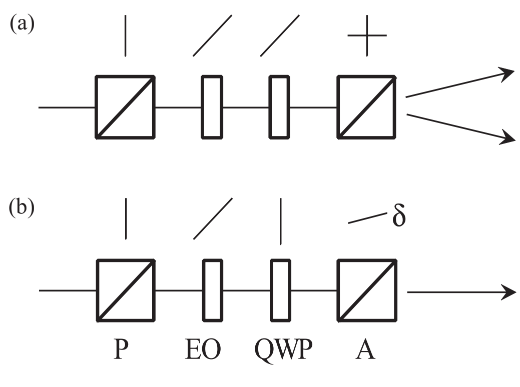

Figure 2. The experimental configuration of the optics in (*a*) balanced detection and (*b*) the OHD method. P, a polarizer; EO, an EO crystal; QWP, a quarter-wave plate; and A, a polarization analyser. The direction of the optical axis of each component is denoted above it. Vertical lines and 45° lines show, respectively, that the optical axes of the components are in the vertical and horizontal directions or in the 45° direction.

which leads to

$$\theta = -\delta + \sqrt{\delta^2 + \frac{I - I_\mathrm{b}}{I_0}} \tag{2}$$

when $|\delta|, |\theta| \ll 1$. Here, I_0 is the incident light intensity, θ is the EO effect contribution to the phase difference, which is proportional to the field, η describes the background contribution due to the intrinsic birefringence of the optics and scattering, and I_b is the background intensity,

$$I_\mathrm{b} = I_0(\eta + \delta^2). \tag{3}$$

The modulation depth is optimized by setting the analyser angle at $\delta \approx \sqrt{\eta}$ [11]. In our set-up, the background contribution from the optical elements between the polarizer and the analyser could be described by $\eta = 1.0 \times 10^{-3}$, which is the extinction ratio of the set-up. Active compensation for the intrinsic birefringence of optical elements was not necessary.

Wu *et al* [2] reported field-linear THz wave detection without the use of a quarter-wave plate. In that case, the local oscillator originates from the polarization rotation of the probe light due to the small birefringence in the ZnTe crystal, and thus the amplitude of the local oscillator cannot be optimized in a controlled manner and is not spatially uniform. By the use of the quarter-wave plate, a spatially uniform local oscillator can be introduced in a controlled fashion.

Following Jiang *et al* [11], the modulation depth, γ, of the measurement is introduced as

$$\gamma \equiv \frac{I_{\theta \neq 0} - I_{\theta = 0}}{I_{\theta \neq 0} + I_{\theta = 0}}. \tag{4}$$

The experimentally obtained δ dependence of the signal modulation depth is plotted in figure 3, which shows close agreement with the theoretical one [11]. In the measurements described later, the orientation of the analyser was set at $\delta = 0.02$ rad, where the modulation depth is almost optimized. To obtain a single image, 30 laser shots were accumulated. Thus the duration required for taking a single image was as short as 30 ms. The experimentally obtained images were

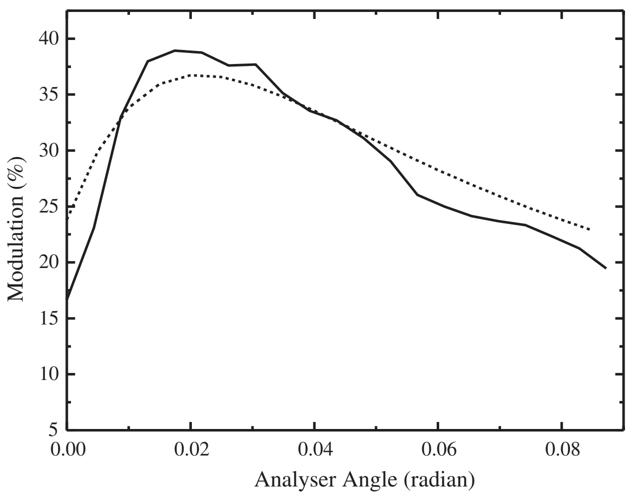

Figure 3. Modulation depth as a function of analyser angle, δ. Solid line shows the experimental result, and the dashed line is the theoretical one with $\eta = 10^{-3}$ and $\theta = 0.025$.

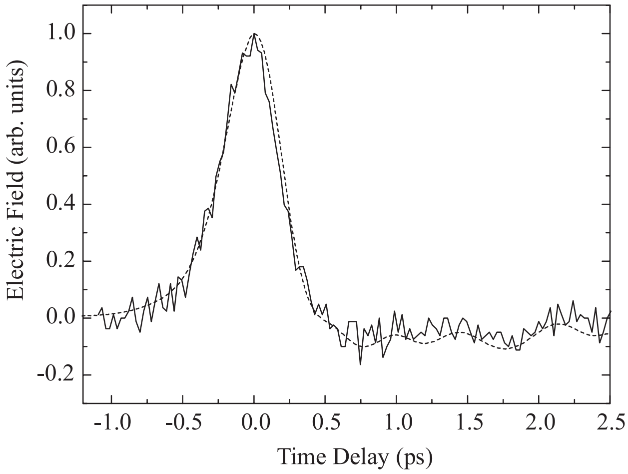

Figure 4. THz temporal waveform obtained using the present OHD imaging method (——) and that obtained using conventional balanced detection (- - - -).

converted to the field images after the measurements using equation (2).

In order to confirm the validity of the present measurement method, we compared the temporal waveform of the THz radiation at the centre of the imaged area, which was reconstructed from a time-scanned sequence of images, with that obtained using the conventional balanced detected EO sampling method at the same position [5]. The result is shown in figure 4, showing that the results obtained using the two methods agree very closely with each other. The waveforms show ringings in the tail due to the free induction decay of water vapour molecules. Since the electric field in this part of the waveform has a small negative value, correct reconstruction of the waveform is not possible using the intensity imaging method and is possible only by means of the field-linear detection method.

3. Results

The time-resolved spatial profiles of the focused electric field of half-cycle pulses on the focal plane obtained with the set-up described above are shown in figure 5. The images correspond to an area of 18.2 mm × 18.2 mm at the position of the EO crystal. At the peak time, which is defined as 0 ps, the profile shows a simple Gaussian-like peak at the centre, as shown in figure 5(*c*). On the other hand, there are time regions before and after the peak, where ring-like profiles are observed, as shown in figures 5(*a*) and (*d*). This feature has been observed previously with THz intensity image measurements [3] and verified by the field images in this study. Jiang and Zhang [15] have reported similar behaviours of few-cycle THz pulses, where multiple-ring structures were observed.

The temporal waveform at each position in the image was reconstructed from a time-scanned image sequence consisting of more than 100 images. By Fourier transforming the field waveform at each position, frequency-resolved spatial distributions of the electric field amplitude were calculated, as shown in figure 6. For better data quality, 4 × 4 pixels were combined and the temporal waveforms of the averaged signal intensity were used for the Fourier analysis.

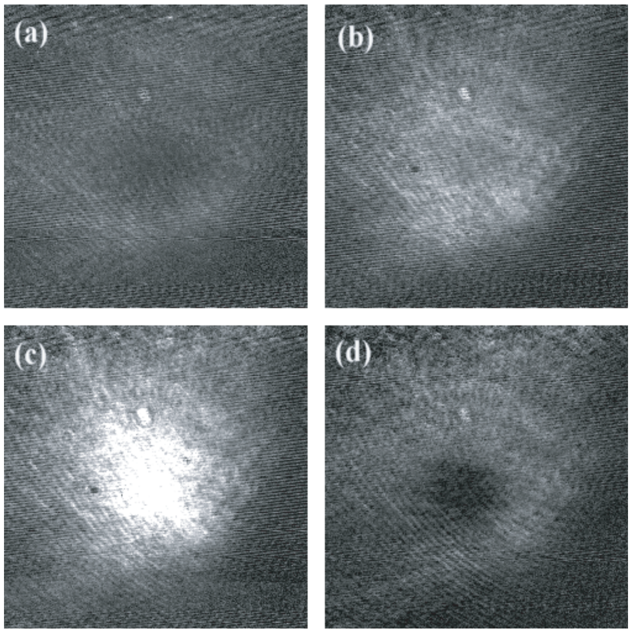

Figure 5. Time-dependence of the two-dimensional spatial profile of the electric field of a focused half-cycle pulse on the focal plane at (*a*) −0.8 ps, (*b*) −0.45 ps, (*c*) 0 ps (peak time), and (*d*) 0.45 ps.

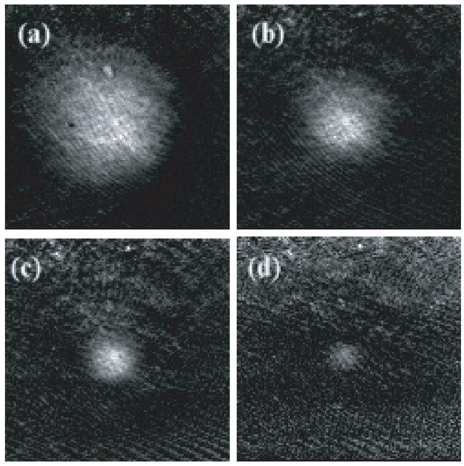

Figure 6. The spatial distribution of the electric field amplitude of (*a*) 0.48 THz, (*b*) 0.99 THz, (*c*) 1.50 THz, and (*d*) 2.16 THz components of the focused THz pulse. The images correspond to an area of 18.2 mm × 18.2 mm at the position of the EO crystal. The amplitude is normalized to the peak value at each frequency. The peak value of image (*d*) is much smaller than that of (*a*), which enhances the relative level of the background noise of the image (*d*).

The present Fourier analysis is possible only using field-linear measurements. Using the conventional detection scheme employing crossed polarizers, the squared field is detected. The Fourier transform of the temporal waveform in that case corresponds to the self-convolution of the spectrum, which should have much more complicated structures compared with the amplitude spectrum itself. It is clearly seen from the frequency dependence of the amplitude distribution, as shown in the figure, that lower-frequency components are focused on a larger area and higher-frequency ones on a smaller area.

For a more quantitative analysis, the beam size of each frequency component was estimated as follows. First, the

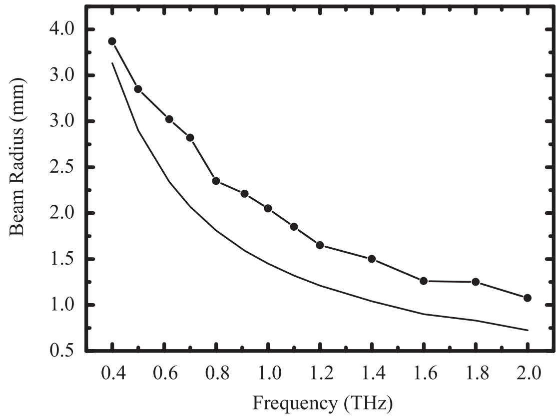

Figure 7. The THz beam sizes obtained from the frequency-dependent amplitude distribution (——●——) in comparison with the beam-waist sizes based on the Gaussian beam model (——).

amplitude profile on the horizontal line that passes through the centre of the image was obtained from each image. Then the $1/e$ radius of the profile was compared with the analytical expression [13]:

$$w_0 = \frac{cf}{A\pi\nu}, \tag{5}$$

which shows the beam-waist size of a focused Gaussian beam of frequency ν in the high-frequency approximation. Here, c is the speed of light, f the focal length, and $A = 10.0$ mm is the beam size of the collimated beam before focusing. This expression shows the diffraction limit for each frequency component. A comparison is shown in figure 7, which exhibits close agreement between the experimental and the Gaussian beam results. Several reports have shown that the essential features of spatio-temporal behaviours of THz pulses can be explained using the Gaussian beam model [3, 13, 16]. In the present beam size comparison, the agreement is very close at low frequencies, which shows that the focusing is almost diffraction-limited. At high frequencies, a deviation as high as 50% of the analytical value is seen, which can be attributed partly to misalignment of optical elements or the limited spatial resolution of the measurement. Although the measurements of the spatial distribution of THz energy or amplitude by scanning a small aperture spatially can suffer from the cutoff effects of the aperture [14, 17], the present method using free-space EO sampling is not affected by such effects.

4. Conclusions

High-speed phase-sensitive time-resolved electric field image detection was achieved by applying the OHD technique for THz imaging measurements using a CCD camera. The introduction of the local oscillator for heterodyne detection was controlled using a quarter-wave plate. By measurement of the time-resolved two-dimensional field distribution of a focused half-cycle THz pulse, a ring-like field distribution in the time-resolved images and almost diffraction-limited focusing in the frequency-resolved images were observed.

Acknowledgment

This study was partly supported by KAKENHI (13450026) from the Japan Society for the Promotion of Science.

References

[1] Mittleman D M, Gupta M, Neelamani R, Baraniuk R G, Rudd J V and Koch M 1999 *Appl. Phys.* B **68** 1085
[2] Wu Q, Hewitt T D and Zhang X-C 1996 *Appl. Phys. Lett.* **69** 1026
[3] Rungsawang R, Ohta K, Tukamoto K and Hattori T 2003 *J. Phys. D: Appl. Phys.* **36** 229
[4] Valdmanis J A, Mourou G and Gabel C W 1982 *Appl. Phys. Lett.* **41** 211
[5] Nahata A, Weling A S and Heinz T F 1996 *Appl. Phys. Lett.* **69** 2321
[6] Eesley G L, Levenson M D and Tolles W M 1978 *J. Quantum Electron.* **14** 45
[7] Levenson M D and Eesley G L 1979 *Appl. Phys.* **19** 1
[8] Ippen E P and Shank C V 1975 *Appl. Phys. Lett.* **26** 92
[9] McMorrow D, Lotshaw W T and Kenney-Wallace G A 1988 *J. Quantum Electron.* **24** 443
[10] Hattori T, Terasaki A, Kobayashi T, Wada T, Yamada A and Sasabe H 1991 *J. Chem. Phys.* **95** 937
[11] Jiang Z, Sun F G, Chen Q and Zhang X-C 1999 *Appl. Phys. Lett.* **74** 1191
[12] Hattori T, Tukamoto K and Nakatsuka H 2001 *Japan. J. Appl. Phys.* **40** 4907
[13] Hattori T, Rungsawang R, Ohta K and Tukamoto K 2002 *Japan. J. Appl. Phys.* **41** 5198
[14] Tukamoto K, Rungsawang R and Hattori T 2003 *Japan. J. Appl. Phys.* **42** 1609
[15] Jiang Z and Zhang X-C 1999 *Opt. Express* **5** 243
[16] You D and Buchsbaum P H 1997 *J. Opt. Soc. Am.* B **14** 1651
[17] Bromage J, Radic S, Agrawal G P and Stroud C R Jr 1998 *J. Opt. Soc. Am.* B **15** 1953